

The Progenitor and Central Engine of short-duration GRB 201006A associated with a coherent radio flash

XIAO TIAN,¹ HOUJUN LÜ,¹ YONG YUAN,² XING YANG,¹ HAOYU YUAN,³ SHUANGXI YI,⁴ WENLONG ZHANG,^{4, 5} AND ENWEI LIANG¹

¹*Guangxi Key Laboratory for Relativistic Astrophysics, Department of Physics, Guangxi University, Nanning 530004, China; lhj@gxu.edu.cn*

²*School of Physics Science And Technology, Wuhan University, No.299 Bayi Road0, Wuhan, 430072 Hubei, China*

³*Department of Astronomy, School of Physics, Huazhong University of Science and Technology, Wuhan, 430074, China*

⁴*School of Physics and Physical Engineering, Qufu Normal University, Qufu 273165, China*

⁵*Key Laboratory of Particle Astrophysics, Institute of High Energy Physics, Chinese Academy of Sciences, Beijing 100049, China*

ABSTRACT

Recently, the detection of a coherent radio flash associated with short GRB 201006A, occurring 76.6 minutes after the burst, has attracted great attention. However, the physical origin of the coherent radio flash remains in debate. By reanalyzing its data observed by Fermi and Swift, we find that an early radio afterglow as the physical origin of the radio flash can be ruled out, but the coherent radio emission seems to be consistent with the hypothesis of a supramassive magnetar as the central engine collapsing into a black hole. Within this scenario, the derived magnetar surface magnetic field (B_p) and the initial spin period (P_0) fall into a reasonable range, but require to prefer a low value of $\eta_R = 10^{-7}$ or 10^{-6} . Moreover, the calculated low- ε value and $E_{\gamma, \text{iso}} - E_p$ correlation of GRB 201006A also support to the progenitor from merger of compact stars. No detected the kilonova emission associated with GRB 201006A to compare with the upper limits of optical observations is also discussed.

Keywords: Gamma-ray bursts

1. INTRODUCTION

The merger of compact binary star systems, comprising either two neutron stars (NS-NS; Paczynski 1986; Eichler et al. 1989) or a neutron star and a black hole (NS-BH; Paczynski 1991), are commonly believed to be the progenitor of short-duration gamma-ray bursts (SGRBs). The simultaneous detection of the gravitational wave event GW170817 and its electromagnetic counterpart (SGRB 170817A and AT2017agf) provides “smoking gun” evidence to support this hypothesis (Abbott et al. 2017a; Abbott et al. 2017b, Goldstein et al. 2017; Savchenko et al. 2017; Zhang et al. 2018), and proves that at least some SGRBs do indeed originate from NS-NS mergers. Nevertheless, the nature of the central engine of SGRB remains under debate. Two leading models of central engine are extensively discussed. One is a hyper-accreting black hole (Popham et al. 1999; Lei et al. 2013; Liu et al. 2017); the other is a rapidly spinning, strongly magnetized neutron star called millisecond magnetar, which powers the outflow of GRBs through its rotation energy (Usov 1992; Thompson 1994; Dai & Lu

1998a,b; Zhang & Mészáros 2001; Metzger et al. 2011; Bucciantini et al. 2012; Lü & Zhang 2014; Lü et al. 2015).

For NS-BH merger, the remnant must be a black hole surrounded by an accretion disk. Within the scenario of NS-NS merger, four possible outcomes of the merger that are dependent on the nascent NS mass (M_p) and its unknown equation of state (EOS) are expected (Lasky et al. 2014; Lü et al. 2015; Li et al. 2016; Gao et al. 2016). One possibility is a black hole when the M_p is much greater than the maximum non-rotating mass (M_{TOV} ; Rosswog et al. 2003; Rezzolla et al. 2011; Ravi & Lasky 2014). Another possible remnant is magnetar. Depending on the relationship between M_p , M_{TOV} , and the maximum gravitational mass (M_{max}), three possible remnants maybe formed for the post-merger evolution of magnetars. Such as, (1) a hyper-massive NS which is supported exclusively by its differential rotation, can survive hundreds of milliseconds (Rosswog et al. 2000; Metzger et al. 2010); (2) a supramassive NS which can be supported by its rigid rotation, can survive from tens of seconds to thousands before collapsing into a black hole (Rowlinson et al. 2010;

Zhang 2013; Lü et al. 2015; Gao et al. 2016; Lü et al. 2017); (3) a stable NS with a much longer lifetime (Dai et al. 2006; Kumar & Zhang 2015; Lü et al. 2018). On the other hand, an optical/infrared transient with near-isotropic (called kilonova) can be generated from the ejected materials and powered by radioactive decay from r-process after binary NS mergers (Li & Paczyński 1998; Metzger et al. 2010; Berger et al. 2013; Yu et al. 2013; Yang et al. 2015; Jin et al. 2016; Yuan et al. 2021; Lü et al. 2022; Troja 2023). A small fraction of SGRBs reported to be associated with kilonova candidates, are already confirmed from the observations (see Metzger 2019 for a review).

From the observational point of view, the X-ray “internal plateaus” with rapid decay at the end of the plateaus in some short GRBs (Rowlinson et al. 2010, 2013; Lü et al. 2015, 2017), are difficult to interpret within the framework of a black hole central engine, but are consistent with a supramassive magnetar as the central engine (Dai et al. 2006; Rowlinson et al. 2010; Gompertz et al. 2013). The rapid decay followed the plateau is suggested to originate from a supramassive magnetar collapsing into a black hole (Zhang 2013; Lü et al. 2015; Kumar & Zhang 2015; Lü et al. 2017). On the other hand, the magnetar model is not the only way to explain X-ray plateau emission, such as the structured jets viewed from off-axis can also explain some X-ray plateau emissions (Beniamini et al. 2020). More interesting, Falcke & Rezzolla (2014) first proposed that a possible radio emission (i.e., fast radio burst) can be produced when a spinning supramassive neutron star loses centrifugal support and collapses to a black hole. Zhang (2014) proposed that this radio emission is possible associated with GRBs. Within this picture, the radio emission would be physically connected to the internal plateau in SGRBs. Bannister et al. (2012) reported that an upper limit of prompt radio emission (i.e., FRB-like event) seems to be consistent with long-duration GRB at the end of plateau emission, but can not be confirmed.

Recently, Rowlinson et al. (2023) claimed that the detection of a coherent radio flash with 5.6σ confidence is associated with the SGRB 201006A. The short radio flash of 144 MHz is detected at 76.6 minutes after the burst trigger time. They proposed that the coherent radio flash is powered by the collapse of a long-lasting supramassive NS as the central engine into a black hole, and the surviving supramassive NS is originated from a binary neutron star merger (Rowlinson et al. 2023). However, Sarin et al. (2024) proposed that the coherent radio emission was powered far from a black hole central engine via synchrotron maser or magnetic reconnection in the jet. In any case, the central engine of

SGRB 201006A associated with the coherent radio flash remains in high debate. If SGRB 201006A is indeed associated with the coherent radio flash, then several questions emerge. What is the progenitor of GRB 201006A? Whether the coherent radio flash could be an early radio afterglow resulting from the interaction between the jet and interstellar medium? What are the physical parameters of supramassive NS as the central engine when we assume that the radio flash is originated from the collapse of a supramassive NS into a black hole?

In this paper, we systematically analyze the observational data of the prompt emission (in Section 2). Then, identifying the progenitor of GRB 201006A by comparing with the other type I and type II GRBs is shown in Section 3. In section 4, we attempt to present that whether the coherent radio flash could be an early radio afterglow (i.e., forward or reverse shock of external shock model), or a supramassive NS as the central engine collapsing into a black hole. The conclusions are drawn in Section 5 with some discussion. Throughout the paper, the convention $Q = 10^x Q_x$ in cgs units and a concordance cosmology with parameters $\Omega_M = 0.30$, $\Omega_\Lambda = 0.70$ and $H_0 = 70 \text{ km s}^{-1} \text{ Mpc}^{-1}$ are adopted.

2. THE OBSERVATIONS AND DATA ANALYSIS

2.1. *Fermi Data Reduction*

At 01:17:52.27 UT on 06 October 2020, the Fermi Gamma-Ray Burst Monitor (GBM) triggered and located GRB 201006A (Hamburg et al. 2020). Fermi/GBM is configured with 12 sodium iodide (NaI) and two bismuth germanate (BGO) scintillation detectors with energy detection ranging from 8keV to 40MeV (Meegan et al. 2009). The corresponding Time-Tagged-Event data were downloaded from the Fermi/GBM public data website¹. Note that more detailed information about light-curve and spectral procedure can be found in Zhang et al. (2016). Here, the light curves of n8, n9 and b1 detectors are shown in Figure 1. We notice that the duration (T_{90}) of GRB 201006A in the energy band 50-300 keV is reported to be 1.7 seconds (Hamburg et al. 2020).

We also extract the time-averaged spectrum of GRB 201006A within the time interval from $T_0 - 0.19 \text{ s}$ to $T_0 + 0.83 \text{ s}$, where T_0 is the trigger time. The background spectra are extracted by selecting two time intervals before and after the burst. We model the background using empirical function (Zhang et al. 2011) and invoke Xspec to fit the spectra. A variety of spectral models can be employed to test the spectral fitting, including power

¹ <https://heasarc.gsfc.nasa.gov/FTP/fermi/data/gbm/daily/>

law (PL), cutoff power law (CPL), blackbody (BB) and Band function (Band), or even the union of any two models. Subsequently, the Bayesian information criteria (BIC)² is employed, revealing that the CPL model exhibits superior goodness of the fits and emerges as the best choice for describing the observed data. Figure 2 shows the fitting results of the CPL model, containing photon spectrum and parameter constraints of the fit. One has peak energy $E_p = 103 \pm 58$ keV and a lower energy spectral index $\alpha = -1.03 \pm 0.30$. According to the spectral analyses, the estimated fluence within $1 - 10^4$ keV energy band during the time interval is $3.12^{+0.58}_{-0.53} \times 10^{-7} \text{ erg cm}^{-2}$.

2.2. Swift Data Reduction

The Burst Alert Telescope (BAT) of Swift also be triggered on October 6, 2020 (Barthelmy et al. 2020). We obtained public BAT data from the Swift archive³ and used the standard HEASOFT (v6.28) tools to process this data. The light curves in different energy bands are extracted by adopting batbinevt (Sakamoto et al. 2008) with fixed 128 ms time-bin, and it consists of a single hard-spike shown in Figure 1. The official website of Swift provides a value of 0.49 ± 0.09 s for the T_{90} in the energy range from 15 to 350 keV.

The Swift X-ray telescope (XRT) began observing the field at 83.9 s after the BAT trigger. We made use of the public data from the Swift archive⁴ (Gropp et al. 2020; Goad et al. 2020). The X-ray light curve seems to be a power-law decay with a decay index of 0.99 (see Figure 6). The Chandra X-ray Observatory also start to observe GRB 201006A at 3.98 days post-trigger (Rouco Escorial et al. 2020), and do not detect an X-ray source within the enhanced Swift-XRT position, but obtain a 3σ limit of $3.6 \times 10^{-4} \text{ cts/s}$ in the 0.5-8 keV energy range.

The Ultra-Violet Optical Telescope (UVOT) began observations of GRB 201006A at 88 seconds after BAT trigger, with no optical afterglow consistent with the XRT position (Marshall et al. 2020). Moreover, the GROWTH India Telescope (GIT), Lowell Discovery Telescope (LDT), and MITSuME are also follow-up to observe this source, but do not find any source in the stacked image, only an upper limit of $r > 20.09$ mag at 17.25 hours, $R > 19.4$ mag at 12.2 hours, $i > 23.8$ mag at

1.44 days after trigger, respectively (Kumar et al. 2020; Ito et al. 2020; Dichiara et al. 2020).

2.3. Estimated the redshift of GRB 201006A

Since no optical counterpart was detected, along with no identified host galaxy within the near-infrared depth range of the X-ray counterpart location for GRB 201006A, one has to estimate the distance of GRB 201006A via dispersion of radio emission. Rowlinson et al. (2023) claimed that the 3.8σ detection significance of radio flash associated with GRB 201006A corresponds to a dispersion measure value of 740-800 pc cm^{-3} when the intrinsic duration is about 5 seconds. They adopted the Macquart correlation (James et al. 2022) to estimate a redshift of GRB 201006A at $z = 0.58 \pm 0.06$ by taking into account the DM range and the contributions of the Galactic to the dispersion measure along the line of sight to GRB 201006A. In this paper, we adopt the redshift $z = 0.58$ to do the calculations.

3. PROGENITOR OF GRB 201006A

Phenomenally, GRBs can be classified into two categories (“long-soft” versus “short-hard”) based on the duration (T_{90}) and spectral hardness of the prompt emission, and the division line is at the duration $T_{90} \sim 2$ s (Kouveliotou et al. 1993; Bromberg et al. 2013). Several lines of observational evidence show that some LGRBs are associated with core-collapse supernovae (SNe; e.g., Woosley 1993; Galama et al. 1998; Stanek et al. 2003; Malesani et al. 2004; Modjaz et al. 2006; Pian et al. 2006), and suggest that LGRBs may originate from the death of massive stars (Type II) (Zhang 2006; Lü et al. 2010; Metzger 2019). In contrast, short GRBs are generally attributed to the merger of two compact stars (Type I), due to that some SGRBs are potentially associated with kilonova and GW radiation rather than SN and typically occur in regions of the host galaxy with little star formation (Zhang 2006; Zhang et al. 2007; Lü et al. 2010; Berger et al. 2013; Jin et al. 2016; Abbott et al. 2017b; Lü et al. 2017; Lamb et al. 2019; Metzger 2019; Troja 2023). However, the measurement of T_{90} is energy and instrument dependent (Qin et al. 2013). Some short-duration GRBs may be from death of massive stars, e.g., GRB 200826A (Ahumada et al. 2021; Zhang et al. 2021; Rossi et al. 2022), or long-duration GRBs are from mergers of two compact stars, e.g., GRB 060614 (Gehrels et al. 2006; Yang et al. 2015), GRB 211211A (Rastinejad et al. 2022; Troja et al. 2022; Yang et al. 2022; Chang et al. 2023; Gompertz et al. 2023), GRB 211227A (Lü et al. 2022; Ferro et al. 2023), GRB 230307A (Dichiara et al. 2023; Sun et al. 2023; Levan et al. 2024; Yang et al. 2024; Du et al. 2024; Zhong et al. 2024).

² The BIC is a criterion for model selection in a limited set of models. The model with the lowest BIC value is the best. The BIC values of different models are presented as 477 (Band), 358 (BB), 293 (CPL), 505 (PL), 369 (Band+BB), 517 (BB+PL), and 304 (BB+CPL).

³ <https://www.swift.ac.uk/archive/selectseq.php?source=obs&tid=95727>

⁴ https://www.swift.ac.uk/xrt_curves/00998907/

Lü et al. (2010) proposed a new phenomenological classification method of GRBs. They introduced a new parameter ε which is defined as

$$\varepsilon = E_{\gamma,\text{iso},52}/E_{\text{p},z,2}^{5/3}, \quad (1)$$

where $E_{\gamma,\text{iso},52}$ is the isotropic burst energy and $E_{\text{p},z,2} = E_{\text{p}}(1+z)/100\text{keV}$ is the rest-frame peak energy. They found that the ε has a clear bimodal distribution (high- and low- ε regions) with division line at $\varepsilon \sim 0.03$, and the low- ε and high- ε regions are corresponding to the mergers of two compact stars (Type I) and death of massive stars (Type II), respectively. Short-duration GRB 201006A with estimated redshift $z = 0.58 \pm 0.06$, has the isotropic energy $E_{\gamma,\text{iso}} = 2.76_{-0.47}^{+0.51} \times 10^{50}\text{erg}$ within $1-10^4$ keV and peak energy $E_{\text{p}} = 103 \pm 58$ keV, respectively. By adopting above method, one can calculate the $\varepsilon \sim 0.012$, and it is located in the low- ε region. The low- ε value of GRB 201006A suggests that it is consistent with Type I population from the compact star mergers (see Figure 3).

Observationally, on the other hand, some empirical correlations among several observed quantities have been claimed (Zhang et al. 2009), such as Amati relation $E_{\gamma,\text{iso}} - E_{\text{p}}$ (Amati et al. 2002). It is found that a majority of long-duration GRBs (Type II) exhibit a positive correlation as $E_{\text{p}} (E_{\text{p},z} \propto E_{\gamma,\text{iso}}^{1/2})$, even the dispersion of the correlation is large, and outliers do exist (Zhang et al. 2009). However, most short-duration GRBs (Type I) are inconsistent with that of long-duration GRBs, and seem to be shallower a little bit for power index (Zhang et al. 2009). In order to test whether GRB 201006A is obeyed the empirical correlation of $E_{\gamma,\text{iso}} - E_{\text{p}}$, we plot GRB 201006A in the $E_{\text{p}} - E_{\gamma,\text{iso}}$ diagram and compare with other Type I and Type II GRBs (see Figure 3). It is found that GRB 201006A deviates the correlation of Type II GRBs, but seems to be more close to Type I GRBs population. In any case, both ε method and Amati relation indicate that the progenitor of GRB 201006A should be originated from the merger of compact stars, e.g., NS-NS or NS-BH. Together with the observed coherent radio emission associated with GRB 201006A, the merger of NS-NS is likely to be the potential candidate of GRB 201006A progenitor.

4. POSSIBLE PHYSICAL ORIGIN OF RADIO FLASH ASSOCIATED WITH GRB 201006A

In this section, we present more details of two possible physical origins of radio flash associated with GRB 201006A, e.g., afterglow origin, and the supramassive NS central engine collapsing into a black hole. Also, we compare with the observations, and discuss the possi-

ble kilonova emission within the hypothesis of NS-NS merger.

4.1. Origin of forward/reverse shock of afterglow?

Recently, Rowlinson et al. (2023) claimed to detect a coherent radio flash which is associated with GRB 201006A with 5.6σ confidence. The short radio flash of 144 MHz with duration of 5 seconds was detected at 76.6 minutes (in observer frame) after the burst trigger time, and the peak flux density of the radio flash was 49 ± 27 mJy with a redshift of 0.58 ± 0.06 . Within the framework of fireball model of GRB, the interaction between relativistic jets and the surrounding medium via synchrotron radiation can give rise to multi-wavelength afterglow (X-ray, optical and radio) emissions of GRBs (Mészáros & Rees 1997; Sari et al. 1998; Gao et al. 2013; Yi et al. 2014). One question is that whether the coherent radio flash is an early radio afterglow of SGRB 201006A from external shock. In this section, we adopt the standard external shock with synchrotron emission afterglow model to calculate the flux of the possible early radio emission.

By considering a standard fireball, it is mainly determined by the initial Lorentz factor (Γ) and total kinetic energy ($E_{\text{K},\text{iso}}$). The interaction between relativistic jet and the ambient medium can produce a pair of shocks (forward and reverse) to propagate into the surrounding medium and the ejecta, respectively. Following our previous work in Yi et al. (2014), the time of crossing the shell by reverse shock is the deceleration time, which can be expressed as

$$t_{\text{dec}} \sim \frac{l(1+z)}{2c\Gamma^{8/3}}, \quad (2)$$

where $l = (3E_{\text{K},\text{iso}}/4\pi n m_p c^2)$ is the Sedov length. The initial total kinetic energy $E_{\text{K},\text{iso}} = E_{\gamma,\text{iso}}(1 - \eta_{\gamma})/\eta_{\gamma}$, where η_{γ} is the radiation efficiency of GRBs. By adopting $\eta_{\gamma} \sim 0.2$, one has $E_{\text{K},\text{iso}} \sim 10^{51}$ erg for GRB 201006A due to $E_{\gamma,\text{iso}} = 2.76_{-0.47}^{+0.51} \times 10^{50}$ erg in γ -ray emission. On the other hand, we also adopt the typical ambient-medium density value of short GRBs ($n = 10^{-2} \text{ cm}^{-3}$) and $\Gamma = 100$ to calculate the afterglow flux, and one has $t_{\text{dec}} \sim 307$ s. The evolution of the light curves of forward shock (FS) and reverse shock (RS) are related to three characteristic frequencies: minimum synchrotron frequency (ν_{m}), cooling frequency (ν_{c}), and self-absorption frequency (ν_{a}). $F_{\nu,\text{max}}$ is the peak flux of spectrum.

(1) In the case of FS, based on the standard afterglow model (Sari et al. 1998; Gao et al. 2013; Yi et al. 2013; Du et al. 2023), at the deceleration time t_{dec} , the characteristic parameters of frequencies for FS emission can

be expressed as:

$$\nu_{m,FS} = 4.1 \times 10^{15} \epsilon_{B,f,-2}^{1/2} \epsilon_{e,-1}^2 n_{-2}^{1/2} \Gamma_2^4 \text{ Hz}, \quad (3)$$

$$\nu_{c,FS} = 7.5 \times 10^{18} \epsilon_{B,f,-2}^{-3/2} n_{-2}^{-5/6} \Gamma_2^{4/3} E_{51}^{-2/3} \text{ Hz}, \quad (4)$$

$$\nu_{a,FS} = 2.9 \times 10^8 \epsilon_{B,f,-2}^{1/5} \epsilon_{e,-1}^{-1} n_{-2}^{3/5} E_{51}^{1/5} \text{ Hz}, \quad (5)$$

$$F_{\nu,max,FS} = 7.8 \times 10^{-5} \epsilon_{B,f,-2}^{1/2} n_{-2}^{1/2} E_{51} D_{L,28}^{-2} \text{ Jy}. \quad (6)$$

Here, we adopt the shock microphysics parameters $\epsilon_e = 0.1$, $\epsilon_{B,f} = 0.01$, and the electron injection spectral index is $p = 2.5$. These four parameters of FS before and after the crossing time can be written as (Mészáros & Rees 1997; Sari et al. 1998; Yi et al. 2014):

(a) $t < t_{dec}$,

$$\nu_{a,FS} \propto t^{\frac{3}{5}}, \nu_{m,FS} \propto t^0, \nu_{c,FS} \propto t^{-2}, F_{\nu,max,FS} \propto t^3, \quad (7)$$

(b) $t > t_{dec}$,

$$\nu_{a,FS} \propto t^0, \nu_{m,FS} \propto t^{-\frac{3}{2}}, \nu_{c,FS} \propto t^{-\frac{1}{2}}, F_{\nu,max,FS} \propto t^0. \quad (8)$$

For non-relativistic phase, it would be $\Gamma - 1 = 1$, where $\Gamma \sim (3E_{K,iso}/32\pi n m_p c^5 t^3)^{1/8}$. After this transition time (the connection time between relativistic phase and non-relativistic phase), the parameters of FS emission should be modified as

$$\nu_{a,FS} \propto t^{\frac{6}{5}}, \nu_{m,FS} \propto t^{-3}, \nu_{c,FS} \propto t^{-\frac{1}{5}}, F_{\nu,max,FS} \propto t^{\frac{3}{5}}. \quad (9)$$

(2) In the case of RS, the four parameters ($\nu_{m,RS}$, $\nu_{c,RS}$, $\nu_{a,RS}$, $F_{\nu,max,RS}$) can be expressed as

$$\nu_{m,RS} = 1.3 \times 10^{12} \epsilon_{B,r,-1}^{1/2} \epsilon_{e,-1}^2 n_{-2}^{1/2} \Gamma_2^2 \text{ Hz}, \quad (10)$$

$$\nu_{c,RS} = 2.4 \times 10^{17} \epsilon_{B,r,-1}^{-3/2} n_{-2}^{-5/6} \Gamma_2^{4/3} E_{51}^{-2/3} \text{ Hz}, \quad (11)$$

$$\nu_{a,RS} = 2.9 \times 10^{11} \epsilon_{B,r,-1}^{1/5} \epsilon_{e,-1}^{-1} n_{-2}^{3/5} \Gamma_2^{8/5} E_{51}^{1/5} \text{ Hz}, \quad (12)$$

$$F_{\nu,max,RS} = 2.5 \times 10^{-2} \epsilon_{B,r,-1}^{1/2} n_{-2}^{1/2} \Gamma_2^2 E_{51} D_{L,28}^{-2} \text{ Jy}. \quad (13)$$

The evolution of these parameters for RS emission are shown in follows.

(a) $t < t_{dec}$,

$$\nu_{a,RS} \propto t^{-\frac{33}{10}}, \nu_{m,RS} \propto t^6, \nu_{c,RS} \propto t^{-2}, F_{\nu,max,RS} \propto t^{\frac{3}{2}}, \quad (14)$$

(b) $t > t_{dec}$,

$$\nu_{a,RS} \propto t^{-\frac{102}{175}}, \nu_{m,RS} \propto t^{-\frac{54}{35}}, \nu_{c,RS} \propto t^{-\frac{54}{35}}, F_{\nu,max,RS} \propto t^{-\frac{34}{35}}. \quad (15)$$

If GRB 201006A originated from the merger of compact stars, the circumburst medium density should be less than 10^{-2} cm^{-3} (Gao et al. 2013; Zhang et al. 2016). Figure 4 shows the numerical calculation of FS

and RS afterglow light curves with different parameters (e.g., n , $\epsilon_{B,f}$, and $\epsilon_{B,r}$) of GRB 201006A in the 144 MHz radio afterglow band, but fixed $\epsilon_e = 0.1$, $p = 2.5$ and $\Gamma = 100$. Note that we allow the microphysics parameter $\epsilon_{B,r}$ to be higher than $\epsilon_{B,f}$ because the outflow is likely magnetized (Zhang et al. 2003). In the left panel of Figure 4, we fixed $\epsilon_{B,f} = 0.01$ and $\epsilon_{B,r} = 0.64$ (Yi et al. 2014), and then plotted the light curves of RS and FS by adopting a variable circumburst medium density, i.e., $n = 10^{-2} \text{ cm}^{-3}$, $n = 10^{-4} \text{ cm}^{-3}$, and $n = 10^{-6} \text{ cm}^{-3}$. In the right panel of Figure 4, we fixed $n = 10^{-2} \text{ cm}^{-3}$, and then adopted different parameters of shock microphysics, i.e., $\epsilon_{B,f} = 10^{-2}, 10^{-3}, 10^{-4}$ for FS model, and $\epsilon_{B,r} = 0.1, 0.64, 0.01$ for RS model. It is found that the brightness of FS and RS emissions strongly depends on the values of selected n (left panel in Figure 4). While, the varying values of ϵ_B seems to be effect a little bit of FS and RS light curves in the early time. Moreover, we also compare the observed radio flash with the theoretical calculations of external shock model (e.g., FS and RS models), and find that the flux of observed radio flash at 76.6 minutes is still much higher than that of any afterglow model. It suggests that an early radio afterglow as the physical origin of radio flash associated with GRB 201006A can be ruled out.

4.2. Originated from the collapse of a supramassive magnetar into a black hole?

A number of previous studies suggested that the X-ray internal plateau following extremely steep decay phase of SGRBs can be consistent with the collapse of a supramassive NS into a black hole (Rowlinson et al. 2010; Zhang 2013; Lü et al. 2015, 2017). Meanwhile, the coherent radio emission is expected to be emitted during the collapse (Bannister et al. 2012; Zhang 2014). Within this picture, coherent radio emission and X-ray plateau emission would be simultaneously produced after GRB prompt emission, but is never observed so far. Rowlinson et al. (2023) proposed that the coherent radio flash associated with GRB 201006A is powered by the collapse of a long-lasting supramassive NS as the central engine into a black hole, even we do not observe a clear plateau emission in the X-ray afterglow of SGRB 201006A. In this section, we try to constrain the physical parameters of supramassive NS, and compare with observations and other Type I GRBs.

Based on the method in Zhang & Mészáros (2001), the total rotation energy of a magnetar is

$$E_{rot} = \frac{1}{2} I \Omega_0^2 \approx 2 \times 10^{52} \text{ erg } M_{1.4} R_6^2 P_{0,-3}^{-2}, \quad (16)$$

where I , Ω_0 , R are the moment of inertia, initial angular frequency, and radius of the NS, respectively.

$M_{1.4} = M/1.4M_\odot$ is the mass of the neutron star. In general, the magnetar can lose its rotational energy via both electromagnetic (L_{EM}) and gravitational wave (L_{GW}) radiations (Zhang & Mészáros 2001; Fan et al. 2013; Lasky & Glampedakis 2016). Here, we assume that the rotation energy loss is dominated by dipole radiation and ignore the contribution from energy loss of gravitational wave. The characteristic spin-down timescale (τ) and spin-down luminosity (L_0) can be written as

$$\tau = 2.05 \times 10^3 I_{45} B_{p,15}^{-2} P_{0,-3}^2 R_6^{-6} \text{ s}, \quad (17)$$

$$L_0 = 1.0 \times 10^{49} B_{p,15}^2 P_{0,-3}^{-4} R_6^6 \text{ erg s}^{-1}, \quad (18)$$

where B_p and P_0 correspond to the surface polar cap magnetic field and initial spin period of magnetar, respectively. In our calculations, we adopt $L_{\text{EM}} \approx L_0$. By considering radiatio efficiency (η_X) in X-ray band, the observed X-ray plateau luminosity can be written as

$$L_X = \eta_X L_0. \quad (19)$$

The X-ray radiation efficiency η_X strongly depends on the injected luminosity L_{EM} , and a larger injection luminosity corresponds to a higher radiation efficiency (Xiao & Dai 2019). From observational point of view, several solid magnetar cases claimed that the efficiency from spin-down luminosity to X-ray emission is as low as 10^{-2} or 10^{-3} , such as X-ray transient CDF-S XT2 (Xue et al. 2019; Xiao & Dai 2019), and GRB 230307A (Sun et al. 2023). In this paper, we adopt a constant η_X and fixed as $\eta_X = 10^{-3}$.

If the coherent radio emission is indeed from the collapse of a supramssive magnetar into a black hole, Zhang (2014) proposed that a supramassive magnetar formed by the merger of two neutron stars may collapse into a black hole within $10^3 - 10^4$ s, and magnetic reconnection of the magnetosphere during collapse will produce a short burst of coherent radio emission. If this is the case, the total magnetosphere energy ($E_{\text{B,iso}}$) released via this magnetic reconnection process is expected to be

$$\begin{aligned} E_{\text{B,iso}} &\approx \int_R^{R_{\text{LC}}} 4\pi r^2 \frac{B_p^2}{8\pi} \left(\frac{r}{R}\right)^{-6} dr \\ &\approx (1/6) B_p^2 R^3 \approx (1.7 \times 10^{47}) B_{p,15}^2 R_6^3 \text{ erg}, \end{aligned} \quad (20)$$

where $R_{\text{LC}} \gg R$ is the light cylinder radius. One can define the conversion efficiency ($\eta_R = E_{\text{R,iso}}/E_{\text{B,iso}}$) which is the fraction of magnetosphere energy converted to coherent radio emission. Here, $E_{\text{R,iso}}$ is the isotropic energy of radio flash, and it can be calculated as

$$E_{\text{R,iso}} = 4\pi D_L^2 f / (1+z), \quad (21)$$

where f is the observed fluence of radio emission.

By applying the above physical process to GRB 201006A, the observed fluence of radio flash associated with GRB 201006A is $245 \pm 135 \text{ Jy ms}$ (Rowlinson et al. 2023), and one can calculate $E_{\text{R,iso}} = (3.06 \pm 1.69) \times 10^{41} \text{ erg}$. Since the parameter of η_R is poor unknown, but from the observational point of view, Moroianu et al. (2023) calculated the solid case for FRB 190425 by invoking blitzar model, and determine the efficiency as low as 2×10^{-6} . Based on Eq.(20), we adopt the variable values of $\eta_R = 10^{-4}, 10^{-5}, 10^{-6}, 10^{-7}$ to estimate the B_p for fixed $R = 10 \text{ km}$, and the results are shown in Table 1. Since we do not observe the X-ray plateau emission of GRB 201006A, and the spin-down timescale (τ) cannot be confirmed. However, one can present the lower limit of τ as the time of coherent radio emission which is also the time of supramassive magnetar collapse into a black hole (t_{col}), namely, $\tau \geq t_{\text{col}} \approx 49$ minutes (in the rest-frame; adopting $z = 0.58$). By combined with Eqs.(17) and (18), one can estimate the lower limit of P_0 for varying η_R , and the results are also shown in Table 1. Figure 5 shows the distribution of B_p and P_0 of GRB 201006A, and compares with other short GRBs taken from Lü et al. (2015). We find that B_p of GRB 201006A for different η_R seems to be one order less than that of other short GRBs. It is a natural explanation with the long-lasting X-ray plateau emission and lower spin-down plateau luminosity. One is worth noting that the initial spin period P_0 is below 0.96 ms which is the breakup spin period limit for a NS (Lattimer & Prakash 2004) for $\eta_R = 10^{-4}, 10^{-5}$, and it suggests that η_R seems to prefer lower values, e.g., $\eta_R = 10^{-6}, 10^{-7}$.

On the other hand, one can derive the upper limits of spin-down plateau luminosity (L_0) for varying $\eta_R = 10^{-4}, 10^{-5}, 10^{-6}, 10^{-7}$. It means that the observed X-ray plateau emission should be existent before the coherent radio emission. Figure 6 (left) shows the upper limit of pseudo-plateau luminosity as a function of time in the rest frame, and then compares with the observed X-ray data from Swift/XRT. It is clear to see that no X-ray plateau emission is observed below L_0 for $\eta_R = 10^{-4}$ and 10^{-5} , but possible be existent for $\eta_R = 10^{-6}$ and 10^{-7} due to insufficient observational data before and after the collapse time. It also supports to prefer a lower values of η_R .

Moreover, the collapse time of GRB 201006A is the longest one by comparing with other short GRBs if its central engine is a supramassive magnetar, and it is another reason to make GRB 201006A as an interesting case. In Figure 6 (right), we also compare the $L_X - t_{\text{col}}$ correlation of GRB 201006A with that of other short GRBs. We find that it also follows the same anti-

correlation with that of other short GRBs, and it also supports that they are sharing the same physical process.

4.3. Possible kilonova emission

The merger of binary neutron stars are typically accompanied by an abundance of electromagnetic transients, such as short GRBs and its afterglow emissions (Rezzolla et al. 2011; Troja et al. 2016), and an optical/infrared transient (called kilonova) powered by radioactive decay from r-process (Li & Paczyński 1998; Metzger et al. 2010; Rezzolla et al. 2011; Hotokezaka et al. 2013; Rowlinson et al. 2013). If the central engine of GRB 201006A is a supramassive magnetar, then, the main power of the possible kilonova emission should no longer be limited to the r-process, but the spin energy of the magnetar is also to be considered (Yu et al. 2013; Metzger & Piro 2014; Gao et al. 2017; Yuan et al. 2021; Sarin et al. 2022; Wang et al. 2024; Ai et al. 2024).

From the observational point of view, several optical telescopes are following-up to observe the GRB 201006A, such as GROWTH-India Telescope (Kumar et al. 2020), MITSuME Akeno (Ito et al. 2020) and Lowell Discovery Telescope (Dichiara et al. 2020), but did not find any new point sources within the enhanced Swift/XRT circle, excepting the upper limits. In order to test whether the upper limits of optical observations can be used to constrain the possible kilonova emission associated with GRB 201006A, we numerically calculate the light curve of kilonova emission in i- and r-band. In our calculations, we adopt the ejecta mass in the range of $M_{\text{ej}} = (10^{-4} - 10^{-2}) M_{\odot}$ which is typical values from numerical simulation of NS-NS mergers (Hotokezaka et al. 2013), a relativistic speed $\beta = (0.1 - 0.3)$, and the opacity $\kappa = (0.1 - 10) \text{ cm}^2 \text{ g}^{-1}$. The total energy of the ejecta and shocked medium can be expressed as $E = (\Gamma - 1)M_{\text{ej}}c^2 + \Gamma E'_{\text{int}}$, where Γ and E'_{int} are the Lorentz factor and the internal energy in the comoving frame, respectively. Based on the energy conservation, $dE_{\text{ej}} = (L_{\text{inj}} - L_{\text{e}})dt$, where L_{e} and L_{inj} are the radiated bolometric luminosity and injection luminosity, respectively. L_{inj} is contributed by spin-down luminosity (L_0) from the magnetar and radioactive power (L_{ra}), namely, $L_{\text{inj}} = \xi L_0 + L_{\text{ra}}$. Here, we adopt $\xi = 0.1$, which is converted efficiency from spin-down luminosity to thermal energy of the ejecta (Zhang & Yan 2011). The equation of full dynamic evolution of the ejecta, the evolution of internal energy in the comoving frame, as well as the evolution of the comoving volume, can be taken in Yu et al. (2013) and Yuan et al. (2021). For the spin-down energy of the magnetar, we adopt the timescale of

energy injection $t = 4600 \text{ s}$ and different initial luminosity of energy injection, e.g., $L_0 = 2.76 \times 10^{46} \text{ erg s}^{-1}$, $L_0 = 2.76 \times 10^{47} \text{ erg s}^{-1}$, and $L_0 = 2.76 \times 10^{48} \text{ erg s}^{-1}$, respectively.

Figure 7 shows the light curves of kilonova emission in i- and r-band with different L_0 , and we find that the expected kilonova emission is much fainter than the upper limit of observed optical data. It means that the possible kilonova emission associated with GRB 201006A is too faint to be detected. So that, the possibility that the central engine is a supramassive NS cannot be ruled out, and it is inconsistent with that of results in Sarin et al. (2024).

5. CONCLUSION AND DISCUSSION

GRB 201006A is a short-duration burst with $T_{90} \sim 1.7 \text{ s}$ in 50-300 keV, and was detected by both Swift and Fermi. The γ -ray light curve consists of a single hard-spike. By extracting the spectra of GRB 201006A, we find that the cutoff power-law model is the best fitting model and gives a soft $E_{\text{p}} = 103 \pm 58 \text{ keV}$. Recently, Rowlinson et al. (2023) claimed that the detection of a coherent radio flash at 76.6 minutes after the burst trigger time of GRB 201006A, and one has to estimate the redshift ($z = 0.58 \pm 0.06$) of GRB 201006A via dispersion of radio emission. So that, the isotropic energy at redshift $z = 0.58$ is estimated as $E_{\gamma, \text{iso}} = 2.76^{+0.51}_{-0.47} \times 10^{50} \text{ erg}$. By calculating $\varepsilon \sim 0.012$ and $E_{\gamma, \text{iso}} - E_{\text{p}}$, we suggest that the progenitor of GRB 201006A is likely to be from merger of compact stars.

However, the physics mechanism behind this coherent radio flash is still in debate. Rowlinson et al. (2023) proposed that the coherent radio flash is powered by the collapse of a long-lasting supramassive magnetar as the central engine into a black hole. Sarin et al. (2024) suggested that the central engine is most likely a black hole, and the coherent radio flash is produced in regions far from the black hole through mechanisms such as a synchrotron maser or magnetic reconnection.

In this paper, we first attempt to test whether the radio flash is caused by an early radio afterglow produced by the synchrotron radiation from the interaction between jet and environmental medium. It is found that an early radio afterglow as the physical origin of the radio flash can be ruled out. Then, within the hypothesis of a supramassive magnetar as the central engine collapsing into a black hole (Rowlinson et al. 2023). We find that the derived magnetar surface magnetic field (B_{p}) and the initial spin period (P_0) fall into a reasonable range, but require to prefer a low value of $\eta_{\text{R}} = 10^{-7}$ or 10^{-6} . Moreover, we numerically calculate the possible kilonova emission in the i-band and r-band by consid-

ering both r-process and magnetar-driven. It is found that the calculated luminosity of kilonova is below the upper limits of optical observations, and it may be too faint to be detected. No detected the kilonova emission associated with GRB 201006A is not contradictory to the supramassive magnetar as the central engine which survived for 49 minutes.

Sarin et al. (2024) dismissed the perspective that the central engine is a millisecond magnetar due to the absence of kilonova observations. However, it is worth noting that the simulated ejecta in their model exhibits a higher mass by comparing with that of binary neutron star mergers in numerical simulations, e.g., $M_{\text{ej}} = (10^{-4} - 10^{-2}) M_{\odot}$ (Hotokezaka et al. 2013). So that, we

believe that a supramassive magnetar remains a potential candidate of the central engine for GRB 201006A, and is consistent with the observations.

6. ACKNOWLEDGMENTS

We acknowledge the use of the public data from the Swift and Fermi Science Data Center. This work is supported by the Guangxi Science Foundation the National (grant No. 2023GXNSFDA026007), the Natural Science Foundation of China (grant Nos. 11922301 and 12133003), and the Program of Bagui Scholars Program (LHJ).

REFERENCES

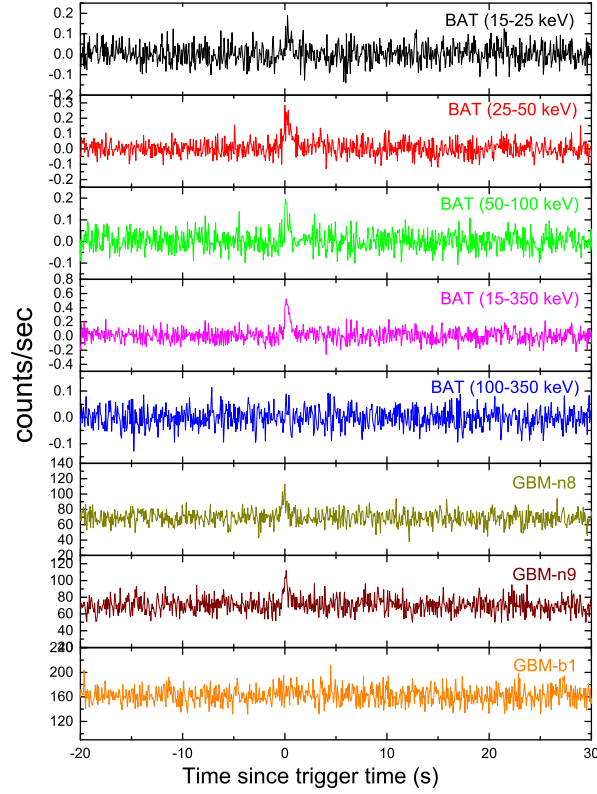
- Abbott, B. P., Abbott, R., Abbott, T. D., et al. 2017a, *ApJL*, 848, L13. doi:10.3847/2041-8213/aa920c
- Abbott, B. P., Abbott, R., Abbott, T. D., et al. 2017b, *PhRvL*, 119, 161101. doi:10.1103/PhysRevLett.119.161101
- Ahumada, T., Singer, L. P., Anand, S., et al. 2021, *Nature Astronomy*, 5, 917. doi:10.1038/s41550-021-01428-7
- Ai, S., Gao, H., & Zhang, B. 2024, arXiv:2405.00638. doi:10.48550/arXiv.2405.00638
- Amati, L., Frontera, F., Tavani, M., et al. 2002, *A&A*, 390, 81. doi:10.1051/0004-6361:20020722
- Bannister, K. W., Murphy, T., Gaensler, B. M., et al. 2012, *ApJ*, 757, 38. doi:10.1088/0004-637X/757/1/38
- Barthelmy, S. D., Cummings, J. R., Gropp, J. D., et al. 2020, *GCN*, No. 28567, 1
- Beniamini, P., Duque, R., Daigne, F., et al. 2020, *MNRAS*, 492, 2847. doi:10.1093/mnras/staa070
- Berger, E., Fong, W., & Chornock, R. 2013, *ApJL*, 774, L23. doi:10.1088/2041-8205/774/2/L23
- Bromberg, O., Nakar, E., Piran, T., et al. 2013, *ApJ*, 764, 179. doi:10.1088/0004-637X/764/2/179
- Bucciantini, N., Metzger, B. D., Thompson, T. A., et al. 2012, *MNRAS*, 419, 1537. doi:10.1111/j.1365-2966.2011.19810.x
- Chang, X.-Z., Lü, H.-J., Yang, X., et al. 2023, *ApJ*, 943, 146. doi:10.3847/1538-4357/aca969
- Dai, Z. G., & Lu, T. 1998a, *A&A*, 333, L87. doi:10.48550/arXiv.astro-ph/9810402
- Dai, Z. G., & Lu, T. 1998b, *PhRvL*, 81, 4301. doi:10.1103/PhysRevLett.81.4301
- Dai, Z. G., Wang, X. Y., Wu, X. F., et al. 2006, *Science*, 311, 1127. doi:10.1126/science.1123606
- Dichiara, S., Cenko, S. B., Troja, E., et al. 2020, *GCN*, No. 28572, 1
- Dichiara, S., Tsang, D., Troja, E., et al. 2023, *ApJL*, 954, L29. doi:10.3847/2041-8213/acf21d
- Du, M., Yi, S.-X., Deng, C.-M., et al. 2023, *Research in Astronomy and Astrophysics*, 23, 115010. doi:10.1088/1674-4527/acee53
- Du, Z., Lü, H., Yuan, Y., et al. 2024, *ApJL*, 962, L27. doi:10.3847/2041-8213/ad22e2
- Eichler, D., Livio, M., Piran, T., et al. 1989, *Nature*, 340, 126. doi:10.1038/340126a0
- Falcke, H. & Rezzolla, L. 2014, *A&A*, 562, A137. doi:10.1051/0004-6361/201321996
- Fan, Y.-Z., Wu, X.-F., & Wei, D.-M. 2013, *PhRvD*, 88, 067304. doi:10.1103/PhysRevD.88.067304
- Ferro, M., Brivio, R., D’Avanzo, P., et al. 2023, *A&A*, 678, A142. doi:10.1051/0004-6361/202347113
- Galama, T. J., Vreeswijk, P. M., van Paradijs, J., et al. 1998, *Nature*, 395, 670. doi:10.1038/27150
- Gao, H., Lei, W.-H., Zou, Y.-C., et al. 2013, *NewAR*, 57, 141. doi:10.1016/j.newar.2013.10.001
- Gao, H., Zhang, B., & Lü, H.-J. 2016, *PhRvD*, 93, 044065. doi:10.1103/PhysRevD.93.044065
- Gao, H., Zhang, B., Lü, H.-J., et al. 2017, *ApJ*, 837, 50. doi:10.3847/1538-4357/aa5be3
- Gehrels, N., Norris, J. P., Barthelmy, S. D., et al. 2006, *Nature*, 444, 1044. doi:10.1038/nature05376
- Goad, M. R., Osborne, J. P., Beardmore, A. P., et al. 2020, *GCN*, No. 28562, 1
- Goldstein, A., Veres, P., Burns, E., et al. 2017, *ApJL*, 848, L14. doi:10.3847/2041-8213/aa8f41
- Gompertz, B. P., O’Brien, P. T., Wynn, G. A., et al. 2013, *MNRAS*, 431, 1745. doi:10.1093/mnras/stt293
- Gompertz, B. P., Ravasio, M. E., Nicholl, M., et al. 2023, *Nature Astronomy*, 7, 67. doi:10.1038/s41550-022-01819-4

- Gropp, J. D., Osborne, J. P., Page, K. L., et al. 2020, GCN, No. 28568, 1
- Hamburg, R., Meegan, C., & Fermi GBM Team 2020, GCN, No. 28564, 1
- Hotokezaka, K., Kiuchi, K., Kyutoku, K., et al. 2013, PhRvD, 87, 024001. doi:10.1103/PhysRevD.87.024001
- Ito, N., Hosokawa, R., Murata, K. L., et al. 2020, GCN, No. 28571, 1
- James, C. W., Prochaska, J. X., Macquart, J.-P., et al. 2022, MNRAS, 509, 4775. doi:10.1093/mnras/stab3051
- Jin, Z.-P., Hotokezaka, K., Li, X., et al. 2016, Nature Communications, 7, 12898. doi:10.1038/ncomms12898
- Kouveliotou, C., Meegan, C. A., Fishman, G. J., et al. 1993, ApJL, 413, L101. doi:10.1086/186969
- Kumar, H., Stanzin, J., Bhalerao, V., et al. 2020, GCN, No. 28573, 1
- Kumar, P. & Zhang, B. 2015, PhR, 561, 1. doi:10.1016/j.physrep.2014.09.008
- Lamb, G. P., Lyman, J. D., Levan, A. J., et al. 2019, ApJL, 870, L15. doi:10.3847/2041-8213/aaf96b
- Lasky, P. D., Haskell, B., Ravi, V., et al. 2014, PhRvD, 89, 047302. doi:10.1103/PhysRevD.89.047302
- Lasky, P. D. & Glampedakis, K. 2016, MNRAS, 458, 1660. doi:10.1093/mnras/stw435
- Lattimer, J. M. & Prakash, M. 2004, Science, 304, 536. doi:10.1126/science.1090720
- Lei, W.-H., Zhang, B., & Liang, E.-W. 2013, ApJ, 765, 125. doi:10.1088/0004-637X/765/2/125
- Levan, A. J., Gompertz, B. P., Salafia, O. S., et al. 2024, Nature, 626, 737. doi:10.1038/s41586-023-06759-1
- Li, A., Zhang, B., Zhang, N.-B., et al. 2016, PhRvD, 94, 083010. doi:10.1103/PhysRevD.94.083010
- Li, L.-X. & Paczyński, B. 1998, ApJL, 507, L59. doi:10.1086/311680
- Liu, T., Gu, W.-M., & Zhang, B. 2017, NewAR, 79, 1. doi:10.1016/j.newar.2017.07.001
- Lü, H.-J., Yuan, H.-Y., Yi, T.-F., et al. 2022, ApJL, 931, L23. doi:10.3847/2041-8213/ac6e3a
- Lü, H.-J., Liang, E.-W., Zhang, B.-B., et al. 2010, ApJ, 725, 1965. doi:10.1088/0004-637X/725/2/1965
- Lü, H.-J. & Zhang, B. 2014, ApJ, 785, 74. doi:10.1088/0004-637X/785/1/74
- Lü, H.-J., Zhang, H.-M., Zhong, S.-Q., et al. 2017, ApJ, 835, 181. doi:10.3847/1538-4357/835/2/181
- Lü, H.-J., Zhang, B., Lei, W.-H., et al. 2015, ApJ, 805, 89. doi:10.1088/0004-637X/805/2/89
- Lü, H.-J., Zou, L., Lan, L., et al. 2018, MNRAS, 480, 4402. doi:10.1093/mnras/sty2176
- Malesani, D., Tagliaferri, G., Chincarini, G., et al. 2004, ApJL, 609, L5. doi:10.1086/422684
- Marshall, F. E., Gropp, J. D., & Swift/UVOT Team 2020, GCN, No. 28565, 1
- Meegan, C., Lichti, G., Bhat, P. N., et al. 2009, ApJ, 702, 791. doi:10.1088/0004-637X/702/1/791
- Metzger, B. D., Giannios, D., Thompson, T. A., et al. 2011, MNRAS, 413, 2031. doi:10.1111/j.1365-2966.2011.18280.x
- Metzger, B. D., Martínez-Pinedo, G., Darbha, S., et al. 2010, MNRAS, 406, 2650. doi:10.1111/j.1365-2966.2010.16864.x
- Metzger, B. D. & Piro, A. L. 2014, MNRAS, 439, 3916. doi:10.1093/mnras/stu247
- Metzger, B. D. 2019, Living Reviews in Relativity, 23, 1. doi:10.1007/s41114-019-0024-0
- Modjaz, M., Stanek, K. Z., Garnavich, P. M., et al. 2006, ApJL, 645, L21. doi:10.1086/505906
- Moroianu, A., Wen, L., James, C. W., et al. 2023, Nature Astronomy, 7, 579. doi:10.1038/s41550-023-01917-x
- Mészáros, P. & Rees, M. J. 1997, ApJ, 476, 232. doi:10.1086/303625
- Paczynski, B. 1986, ApJL, 308, L43. doi:10.1086/184740
- Paczynski, B. 1991, AcA, 41, 257
- Pian, E., Mazzali, P. A., Masetti, N., et al. 2006, Nature, 442, 1011. doi:10.1038/nature05082
- Popham, R., Woosley, S. E., & Fryer, C. 1999, ApJ, 518, 356. doi:10.1086/307259
- Qin, Y., Liang, E.-W., Liang, Y.-F., et al. 2013, ApJ, 763, 15. doi:10.1088/0004-637X/763/1/15
- Rastinejad, J. C., Gompertz, B. P., Levan, A. J., et al. 2022, Nature, 612, 223. doi:10.1038/s41586-022-05390-w
- Ravi, V. & Lasky, P. D. 2014, MNRAS, 441, 2433. doi:10.1093/mnras/stu720
- Rezzolla, L., Giacomazzo, B., Baiotti, L., et al. 2011, ApJL, 732, L6. doi:10.1088/2041-8205/732/1/L6
- Rossi, A., Rothberg, B., Palazzi, E., et al. 2022, ApJ, 932, 1. doi:10.3847/1538-4357/ac60a2
- Rosswog, S., Davies, M. B., Thielemann, F.-K., et al. 2000, A&A, 360, 171. doi:10.48550/arXiv.astro-ph/0005550
- Rosswog, S., Ramirez-Ruiz, E., & Davies, M. B. 2003, MNRAS, 345, 1077. doi:10.1046/j.1365-2966.2003.07032.x
- Rouco Escorial, A., Fong, W., Schroeder, G., et al. 2020, GCN, No. 28598, 1
- Rowlinson, A., O'Brien, P. T., Metzger, B. D., et al. 2013, MNRAS, 430, 1061. doi:10.1093/mnras/sts683
- Rowlinson, A., O'Brien, P. T., Tanvir, N. R., et al. 2010, MNRAS, 409, 531. doi:10.1111/j.1365-2966.2010.17354.x
- Rowlinson, A., de Ruiter, I., Starling, R. L. C., et al. 2023, arXiv:2312.04237. doi:10.48550/arXiv.2312.04237
- Sakamoto, T., Barthelmy, S. D., Barbier, L., et al. 2008, ApJS, 175, 179. doi:10.1086/523646

- Sari, R., Piran, T., & Narayan, R. 1998, *ApJL*, 497, L17.
doi:10.1086/311269
- Sarin, N., Omand, C. M. B., Margalit, B., et al. 2022, *MNRAS*, 516, 4949. doi:10.1093/mnras/stac2609
- Sarin, N., Clarke, T. A., Magnall, S. J., et al. 2024, arXiv:2404.08048. doi:10.48550/arXiv.2404.08048
- Savchenko, V., Ferrigno, C., Kuulkers, E., et al. 2017, *ApJL*, 848, L15. doi:10.3847/2041-8213/aa8f94
- Stanek, K. Z., Matheson, T., Garnavich, P. M., et al. 2003, *ApJL*, 591, L17. doi:10.1086/376976
- Sun, H., Wang, C.-W., Yang, J., et al. 2023, arXiv:2307.05689. doi:10.48550/arXiv.2307.05689
- Thompson, C. 1994, *MNRAS*, 270, 480.
doi:10.1093/mnras/270.3.480
- Troja, E., Sakamoto, T., Cenko, S. B., et al. 2016, *ApJ*, 827, 102. doi:10.3847/0004-637X/827/2/102
- Troja, E., Fryer, C. L., O'Connor, B., et al. 2022, *Nature*, 612, 228. doi:10.1038/s41586-022-05327-3
- Troja, E. 2023, *Universe*, 9, 245.
doi:10.3390/universe9060245
- Usov, V. V. 1992, *Nature*, 357, 472. doi:10.1038/357472a0
- Wang, H., Beniamini, P., & Giannios, D. 2024, *MNRAS*, 527, 5166. doi:10.1093/mnras/stad3560
- Woosley, S. E. 1993, *A&AS*, 97, 205
- Xiao, D. & Dai, Z.-G. 2019, *ApJ*, 878, 62.
doi:10.3847/1538-4357/ab12da
- Xue, Y. Q., Zheng, X. C., Li, Y., et al. 2019, *Nature*, 568, 198. doi:10.1038/s41586-019-1079-5
- Yang, B., Jin, Z.-P., Li, X., et al. 2015, *Nature Communications*, 6, 7323. doi:10.1038/ncomms8323
- Yang, J., Ai, S., Zhang, B.-B., et al. 2022, *Nature*, 612, 232. doi:10.1038/s41586-022-05403-8
- Yang, Y.-H., Troja, E., O'Connor, B., et al. 2024, *Nature*, 626, 742. doi:10.1038/s41586-023-06979-5
- Yi, S.-X., Wu, X.-F., & Dai, Z.-G. 2013, *ApJ*, 776, 120.
doi:10.1088/0004-637X/776/2/120
- Yi, S.-X., Gao, H., & Zhang, B. 2014, *ApJL*, 792, L21.
doi:10.1088/2041-8205/792/1/L21
- Yu, Y.-W., Zhang, B., & Gao, H. 2013, *ApJL*, 776, L40.
doi:10.1088/2041-8205/776/2/L40
- Yuan, Y., Lü, H.-J., Yuan, H.-Y., et al. 2021, *ApJ*, 912, 14.
doi:10.3847/1538-4357/abedb1
- Zhang, B.-B., Zhang, B., Liang, E.-W., et al. 2011, *ApJ*, 730, 141. doi:10.1088/0004-637X/730/2/141
- Zhang, B.-B., Zhang, B., Sun, H., et al. 2018, *Nature Communications*, 9, 447. doi:10.1038/s41467-018-02847-3
- Zhang, B.-B., Uhm, Z. L., Connaughton, V., et al. 2016, *ApJ*, 816, 72. doi:10.3847/0004-637X/816/2/72
- Zhang, B.-B., Liu, Z.-K., Peng, Z.-K., et al. 2021, *Nature Astronomy*, 5, 911. doi:10.1038/s41550-021-01395-z
- Zhang, B., Kobayashi, S., & Mészáros, P. 2003, *ApJ*, 595, 950. doi:10.1086/377363
- Zhang, B., Lü, H.-J., & Liang, E.-W. 2016, *SSRv*, 202, 3.
doi:10.1007/s11214-016-0305-9
- Zhang, B. 2006, *Nature*, 444, 1010. doi:10.1038/4441010a
- Zhang, B. & Mészáros, P. 2001, *ApJL*, 552, L35.
doi:10.1086/320255
- Zhang, B., Zhang, B.-B., Liang, E.-W., et al. 2007, *ApJL*, 655, L25. doi:10.1086/511781
- Zhang, B., Zhang, B.-B., Virgili, F. J., et al. 2009, *ApJ*, 703, 1696. doi:10.1088/0004-637X/703/2/1696
- Zhang, B. 2014, *ApJL*, 780, L21.
doi:10.1088/2041-8205/780/2/L21
- Zhang, B. 2013, *ApJL*, 763, L22.
doi:10.1088/2041-8205/763/1/L22
- Zhang, B. & Yan, H. 2011, *ApJ*, 726, 90.
doi:10.1088/0004-637X/726/2/90
- Zhong, S.-Q., Li, L., Xiao, D., et al. 2024, *ApJL*, 963, L26.
doi:10.3847/2041-8213/ad2852

Table 1. The derived parameters or upper limits of the magnetar for different efficiency η_R .

η_R	P_0	$B_{p,15}$	L_0
	(ms)	(G)	(erg s $^{-1}$)
10^{-7}	5.06 \uparrow	4.25	$2.76 \times 10^{47} \downarrow$
10^{-6}	1.60 \uparrow	1.34	$2.76 \times 10^{48} \downarrow$
10^{-5}	0.51 \uparrow	0.42	$2.76 \times 10^{49} \downarrow$
10^{-4}	0.16 \uparrow	0.13	$2.76 \times 10^{50} \downarrow$

**Figure 1.** Swift/BAT and Fermi/GBM light curves of GRB 201006A in different energy bands with a 128 ms time-bin.

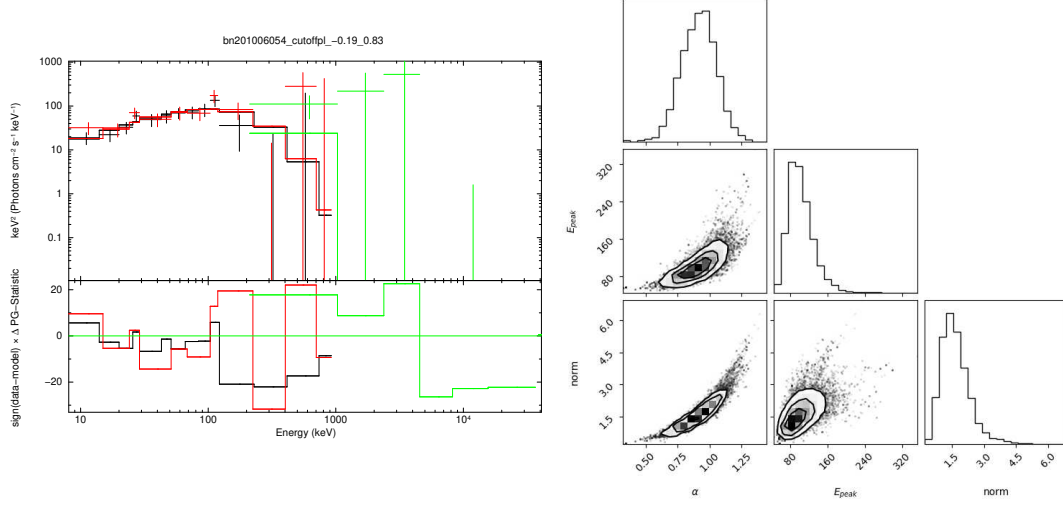


Figure 2. Spectral fit results of GRB 201006A from $T_0 - 0.19$ s to $T_0 + 0.83$ s with the CPL model for Fermi/GBM, including the photon spectrum (left) and parameter constraints (right) of the CPL fit.

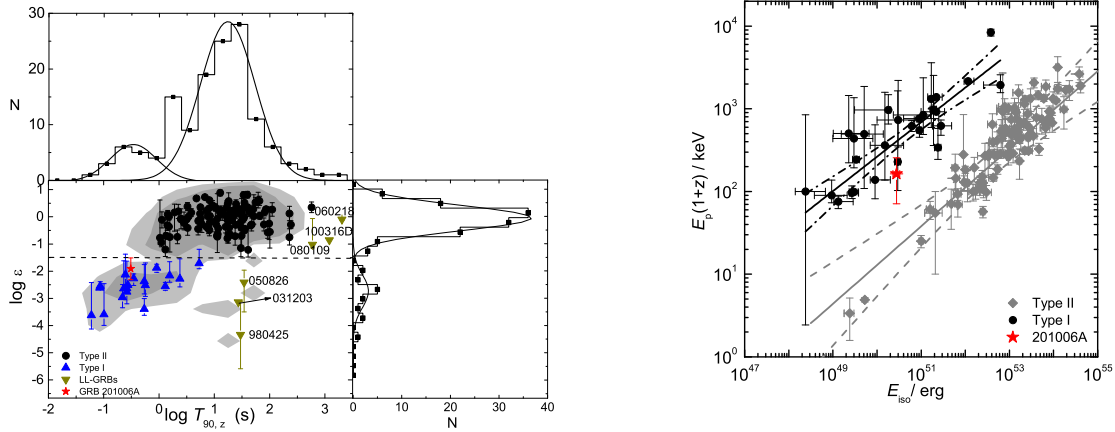


Figure 3. Left: 1D and 2D distributions of GRBs samples in $T_{90} - \epsilon$ space. The dashed line indicates $\epsilon = 0.03$, and the data come from Lü et al. (2010). Right: $E_p - E_{\gamma, \text{iso}}$ correlation diagram. Gray diamonds and black dots correspond to type II and type I GRBs, which are from Amati et al. (2002) and Zhang et al. (2009). The red star indicates GRB 201006A. The black and gray solid lines represent the best-fit lines, and dashed lines represent the 3σ confidence bands.

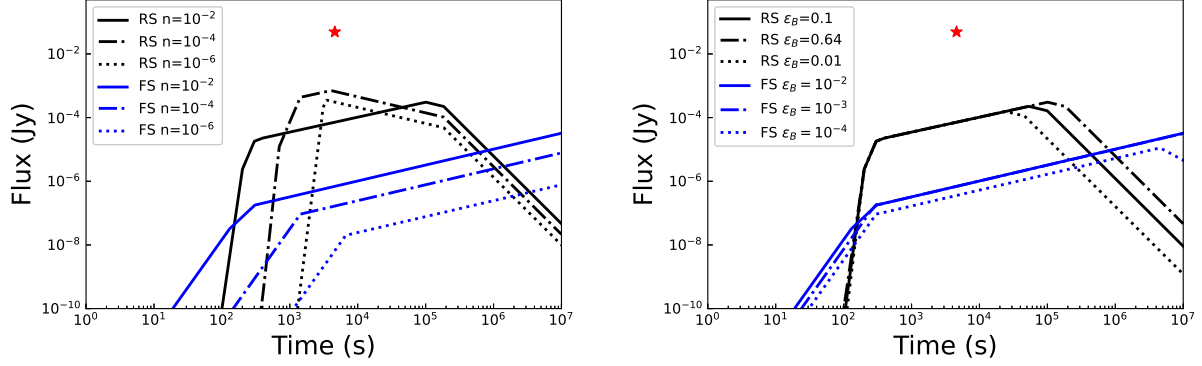


Figure 4. Numerical calculation of FS and RS afterglow light curves in radio band of GRB 201006A. The model parameters: $\epsilon_e = 0.1$, $p = 2.5$ and $\Gamma = 100$. Left: The case of FS (blue) and RS (black) light curves at different circumburst medium densities. Different shock microphysical parameters ϵ_B are adopted: $\epsilon_{B,f} = 0.01$ for FS model and $\epsilon_{B,r} = 0.64$ for RS model. Right: The case of FS and RS light curves under different shock microphysics parameters ϵ_B . We apply the typical circumburst density value ($n = 10^{-2} \text{ cm}^{-3}$) of SGRBs to calculate the afterglow flux. The red star represents the observed peak flux density 49 ± 27 mJy of the radio flash with a redshift of 0.58 ± 0.06 (Rowlinson et al. 2023).

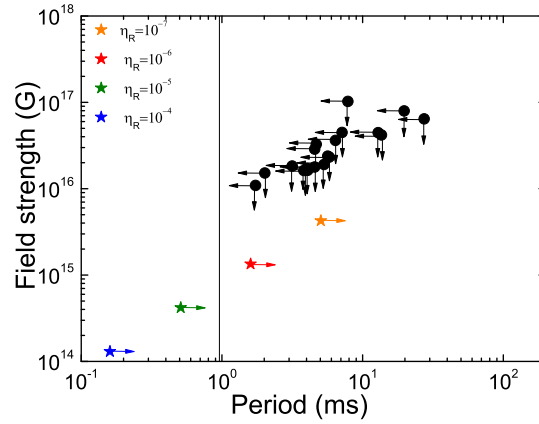


Figure 5. Inferred magnetar parameters. Initial spin period P_0 vs. surface polar cap magnetic field strength B_p derived by short GRBs with internal plateaus (black dots) from Lü et al. (2015). The stars are GRB 201006A in case $\eta_R = 10^{-4}, 10^{-5}, 10^{-6}$ and 10^{-7} , respectively. The vertical solid line is the breakup spin period limit for a neutron star (Lattimer & Prakash 2004).

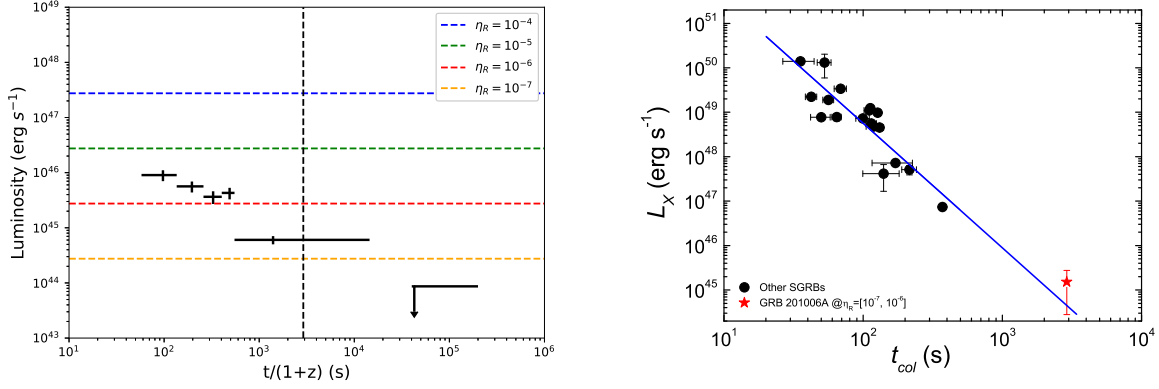


Figure 6. Left: The inferred X-ray plateau luminosity at various radiation efficiencies η_R . The data points are taken from the swift website and the black dashed line represents the burst time of radio flash (in rest-frame). Right: $L_X - t_{col}$ anti-correlation for short GRBs with internal plateaus. The black dots indicate the samples from Lü et al. (2015), and the red star is GRB 201006A.

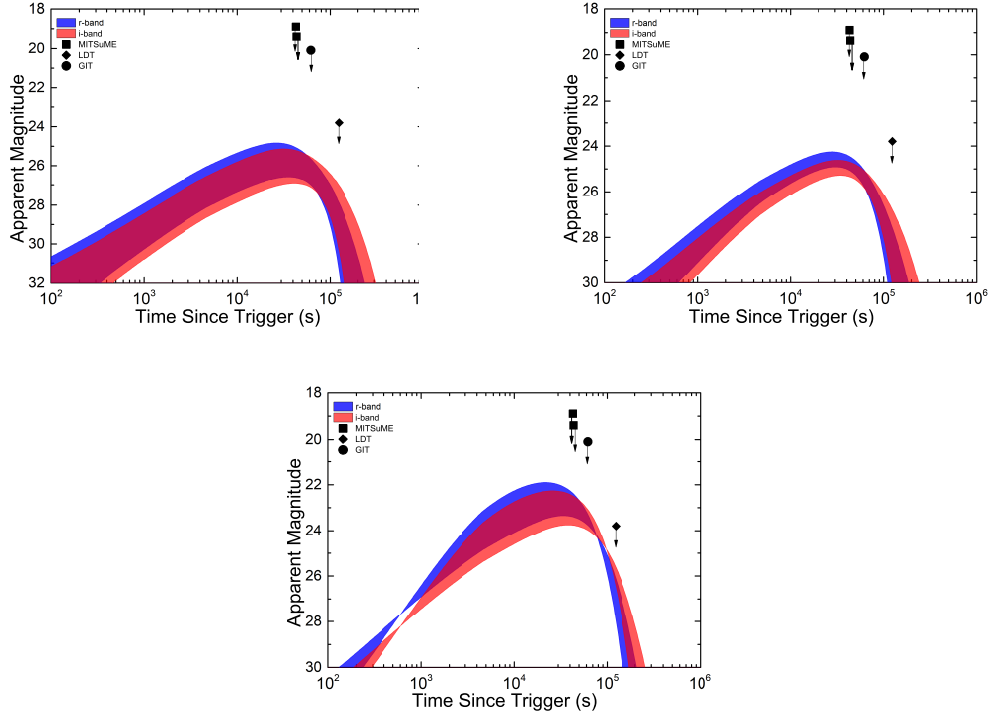


Figure 7. Magnetar-driven kilonova light curves in i-band (red) and r-band (blue). From left to right, the kilonova light curves under three different initial injection luminosity, $L_0 = 2.76 \times 10^{46}$ erg s⁻¹, $L_0 = 2.76 \times 10^{47}$ erg s⁻¹ and $L_0 = 2.76 \times 10^{48}$ erg s⁻¹ respectively. The other parameters can be ranged of in $M_{ej} = (10^{-4} - 10^{-2}) M_{\odot}$, $\beta = (0.1 - 0.3)$, and $\kappa = (0.1 - 10)$ cm² g⁻¹. The black square, circle and diamond correspond to the upper limits of optical observations.